Cavitation Characteristics in Ultrasonic Soldering and the Erosion Effect

Cavitation is fundamentally responsible for the removal of the oxide layer during ultrasonic soldering, and its characteristics are studied with high-speed photography

BY Z. LI, Z. XU, B. ZHANG, AND J. YAN

Abstract

In this work, the cavitation characteristics of the solder sonocapillary action during ultrasonic soldering were studied by a high-speed camera. The effects of ultrasonic power and time on the acoustic pressure, cavitation characteristics, and erosion effects were also investigated. Results showed that cavitation occurred throughout the entire sonocapillary action. Two kinds of bubble structures were observed. The steady bubbles had large sizes and long life periods. The transient bubbles had small sizes and short life periods. The steady bubbles preferentially appeared at the primary filling stage, while the transient bubbles dominated the entire cavitation field. The sonocapillary action was divided into the primary filling stage, the intermediate filling stage, and the completion filling stage. The primary filling stage had low acoustic pressure but high bubble density because the air content in the solder was high and some additional air entered the solder through the triple interface caused by ultrasonic vibration. Higher ultrasonic power resulted in stronger cavitation and, thus, better erosion effect on the substrate.

Keywords

- Ultrasonic Soldering
- Sonocapillary
- Cavitation Bubble
- Acoustic Pressure
- Erosion
- Oxide Layer

Introduction

Ultrasonic soldering can be operated directly in the air without any gas protection (Ref. 1). It does not require flux, thus saving costs and reducing pollution (Ref. 2). Ultrasonic soldering is a promising method for joining various kinds of materials, and it has been used to join Al alloys (Refs. 3, 4), Mg alloys (Refs. 5, 6), Ti alloys (Ref. 7), composite materials (Refs. 8, 9), ceramics (Refs. 10–12), glass (Ref. 13), sapphire (Ref. 14), and even graphite (Ref. 15).

Ultrasonic soldering dates to the 1960s. The earliest ultrasonic soldering was ultrasonic bath soldering. By ultrasonic bath soldering, Jenkins (Ref. 16) and Gunkel (Ref. 17) soldered Al/Cu heat exchangers using Zn5Al solder. However, Gunkel (Ref. 17) found that a joint can only be formed when it is located 38–50 mm (1.496–1.968 in.) beneath the solder surface. Also, ultrasonic bath soldering requires a large solder volume, thus causing low ultrasonic energy density in solder. During soldering, the nonsoldering area of the specimen is also immersed in solder, causing harmful erosion and contamination. Thereafter, a series of ultrasonic soldering methods were developed. During soldering, Tamura et al. (Ref. 18) assembled the sonotrode close to the Zr-based glass and reported that an ultrasonic time of 900 s resulted in good wetting of Sn–Cu–Ni solder to Zr-based glass. However, the solder volume was still large, and the erosion of the nonsoldering area could not be avoided in their work. The density of ultrasonic energy in solder can be improved by reducing the solder volume. Therefore, some methods requiring only a tiny solder droplet were invented (Refs. 19, 20). One typical example is ultrasonic iron soldering, which is still used today.

Compared with ultrasonic bath soldering, all the above-mentioned methods can improve the density of ultrasonic energy. However, none of them can avoid the erosion of the sonotrode. Intense cavitation could occur near the sonotrode after it is immersed in solder; the erosion greatly reduces its life. Dong et al. (Ref. 21) reported that a TC4 sonotrode was

https://doi.org/10.29391/2024.103.023

seriously eroded when it was immersed in liquid 7050 Al at 700°C (1292°F) for 3 h.

In 2009, Yan et al. (Ref. 22) invented a new substrate-initiated ultrasonic soldering method. It had several advantages. First, the sonotrode was no longer immersed in solder, which could avoid erosion damage and greatly prolong the sonotrode's usage life. Second, the soldering efficiency was high. During this method, the capillary filling of the solder was very fast, and a joint could be obtained within an extremely short time (Refs. 23, 24). Third, the solder had a small volume, and a high utilization rate of ultrasonic energy could be guaranteed.

The mechanism for all these ultrasonic soldering methods is cavitation. Cavitation is a phenomenon where tiny gas bubbles in liquid could undergo repeated nucleation and growth and collapse violently under the action of ultrasound (Refs. 25–30). The collapse of cavitation bubbles could produce instantaneous high temperatures (Refs. 30–33) and pressure (Ref. 34) and micro-jet with high velocity (Refs. 35–37). Having undergone cavitation, the material can be broken within a short period (Ref. 38). During ultrasonic soldering, cavitation at the solder/substrate interface is fundamentally responsible for the removal of the oxide layer on the substrate (Ref. 39), meaning that the cavitation in the liquid solder can largely determine the joint quality. For an Al alloy, its surface oxide layer must be completely removed before a sound joint can form. Our group studied the relationship between cavitation and joint quality in detail (Refs. 25, 39). Results showed that the cavitation intensity of Sn solder is low inside a 0.8 mm-wide joint clearance (Ref. 25). Thus, it needs a longer time for cavitation to completely remove the oxide layer (Ref. 39). By contrast, the cavitation intensity inside a 0.2 mm (0.008 in.)-wide joint clearance is higher (Ref. 25), thereby needing a much shorter time to remove the oxide layer (Ref. 39). Also, when a liquid Sn droplet spreads on Al, the oxide layer of Al at the spreading front is difficult to remove due to a noncavitation situation (Ref. 40).

Therefore, cavitation is one of the core phenomena of ultrasonic soldering. However, since the invention of ultrasonic soldering, most of the openly published works have focused on the effects of solder type, substrate type, and soldering parameters on the microstructure and mechanical properties of soldered joints (Refs. 41–44). Other than ours (Refs. 40, 45), few works have studied the cavitation phenomena during ultrasonic soldering.

Ultrasonic soldering is also one type of ultrasonic melt processing. So far, some literature has studied cavitation during ultrasonic melt processing, during which the main method is synchrotron radiation x-ray imaging since the liquid solders are opaque. For example, Huang et al. (Ref. 46) studied the cavitation bubbles in Al–10 wt-% Cu and reported that most of the bubbles concentrated near the sonotrode surface. They also reported that the bubbles were larger than those in water because of the higher ultrasonic intensity in Al–10 wt-% Cu liquid. Mirihanage et al. (Ref. 47) reported that the nano Al_2O_3 particles significantly increased the bubble density. Xu et al. (Ref. 48) reported that the cavitation bubbles in Al–10 wt-% Cu had an average radius of 15.3 ± 0.5 μm. Mi's group (Refs. 49–51) studied the cavitation bubbles in liquid metal in detail and studied their effects on microstructure fragmentation during solidification.

The cavitation mechanism during ultrasonic soldering differs significantly from those that occur in ultrasonic melt processing due to the following reasons: 1. The liquid solder is thin during ultrasonic soldering. The clearances between substrates are narrow, commonly smaller than 1 mm (0.039 in.) (Ref. 39). Thus, cavitation during ultrasonic soldering occurs in some extremely thin liquid layers; 2. Ultrasonic soldering involves the propagation of ultrasound waves in solid substrate and liquid solder. The reflection or interference of ultrasound waves inevitably influences the energy transmitted from substrate to solder; and 3. Most of the solder directly contacts the air during its filling, which is quite different from the previous cavitation observation experiment (Ref. 27).

Thus, the cavitation characteristics during the ultrasonic soldering process were studied in this work, aiming to reveal the removal mechanism of the oxide layer on the substrate surface. The main research objects in this work were: 1. The cavitation characteristic during the solder filling process. Such a process was realized by using a high-speed camera. The main cavitation structures were discovered. Also, the variations of cavitation using different parameters were obtained; 2. Acoustic pressure in the solder and its relationship with cavitation. The acoustic pressure was predicted by Fluent software, and the effects of soldering parameters on the acoustic pressure were analyzed; 3. Erosion effect of solder on the substrate. The erosion characteristics after the solder filling process were observed, and the effects of the soldering parameters on the erosion effects were also analyzed. This work is of great significance to reveal the fundamental mechanism of ultrasonic soldering.

Experimental and Simulation

Substrate and Bolder

Pure Al, provided by the Northeast Light Alloy Co. Ltd., was used as the substrate. The density, elastic modulus, and Poisson's ratio of pure Al are 2.7 g/cm^3, 68.9 GPa, and 0.31, respectively. The dimensions of the substrates were 50 mm × 10 mm (0.394 in.) × 3 mm (0.118 in.). The substrate sheets were polished with 500# emery papers and ultrasonically cleaned in acetone.

Under conventional conditions, the surface of the metal substrate is covered with an oxide layer. The purpose of erosion is to remove such an oxide layer. A sufficient erosion effect can completely remove the oxide layer and result in good joint strength. Therefore, it is necessary to study the erosion in ultrasonic soldering. To study the erosion effect more clearly, the substrates were anodic oxidized. A thicker Al_2O_3 layer 5 μm thick was fabricated on the pure Al sheet. During the anodic oxidation process, the electrolytic solution was 15 g/L $H_2C_2O_4$. Pure Al served as the positive pole, and a Cu sheet was used as the negative pole. The anodizing current, voltage, and time were 0.3 A, 53.6 V, and 3 min, respectively. During soldering, the solder was pure Sn. The melting point of pure Sn is 231°C (448°F). The density and

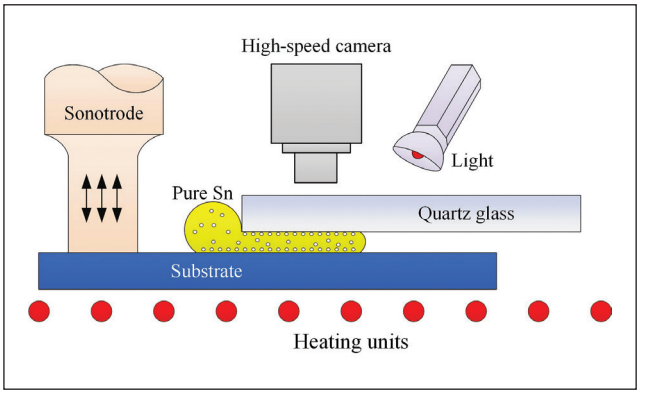

Fig. 1 — Schematic of the cavitation recording experiment.

viscosity of pure Sn at 250°C (482°F) was 7.3 g/cm^3 and 2.64 mPa·s (Ref. 40).

Solder Filling Experiment

The ultrasonic soldering equipment was a self-designed system called UPM-UP1010A01. The sonotrode was made of TC4 alloy and had a diameter of 20 mm (0.787 in.). The sonotrode was operated at 20 kHz and had a maximum output power (Pm) of 1000 W. Three output amplitudes were used, namely 4 µm (Mode I, 333.3 W), 5 µm (Mode II, 666.7 W), and 6 µm (Mode III, 1000 W). The sonotrode was kept against the substrate at a pressure of 0.2 MPa during solder filling. The clearance width between the substrate was kept at 0.2 mm. Figure 1 shows a schematic of the solder filling experiment. The temperature was 250°C, which was measured by a thermocouple fixed on the lower substrate. Pure Sn was put near the substrate clearance in advance. A transparent quartz glass was used as the upper substrate, providing good visual access to the solder/glass interface. We could clearly observe the cavitation bubble characteristics during the solder filling process by focusing the camera's field of view on the solder/glass interface. A high-speed camera, Phantom V12.1 equipped with a macro lens (Tokina 100 mm f2.8 Macros), was used to record the solder filling action and cavitation bubbles. The images were taken using acquisition rates of 5000 fps and 20,000 fps. The recording time limits were all set to 2 s. Three tests were repeated for each experiment condition.

To study the erosion effect on the Al substrate, the samples used in previous visualization results were immersed into a 20% diluted HNO_3 solution to remove the pure Sn solder. Then the eroded substrate was cleaned in acetone and dried. The erosion morphology of the eroded Al was observed on a scanning electron microscope (SEM, Quanta 200FEG).

Simulation

During the experiment, ultrasonic waves were first transmitted in the pure Al by the ultrasonic sonotrode, and then they propagated into the liquid solder. Thus, the vibration

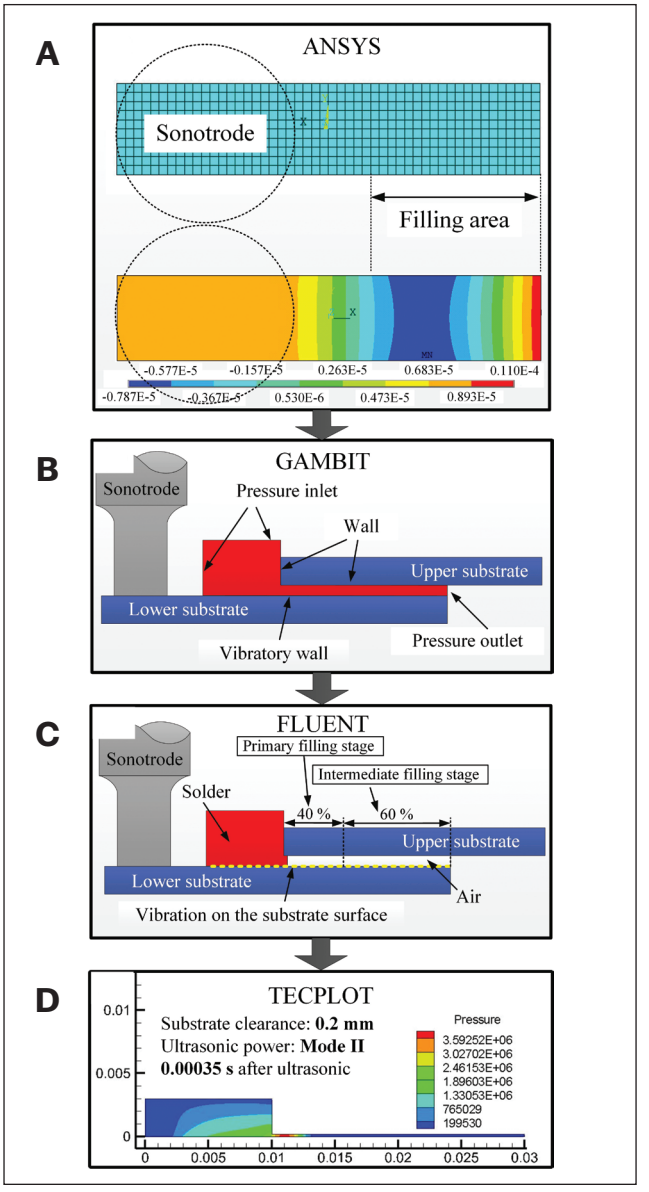

Fig. 2 — Schematic of simulation: A — Calculating the vibration on Al; B — defining boundary conditions in Gambit; C — loading the vibration by FLUENT; D — data acquisition by Tecplot.

response of pure Al under ultrasonic directly affected the acoustic pressure in the solder, which greatly affected the solder filling action and cavitation characteristic. Therefore, the vibration intensity and acoustic pressure were simulated. The vibration amplitude on the substrate was calculated using the harmonic response analysis module of ANSYS software. Then, a solid model was built by Gambit. Thirdly, the solid model was introduced in Fluent software, and the vibration characteristics were coupled to the boundary condition to calculate the filling of the solder and the acoustic pressure in the solder. At last, the calculated data was read by Tecplot. A detailed description of the function of each software can be found in our previous work (Ref. 45).

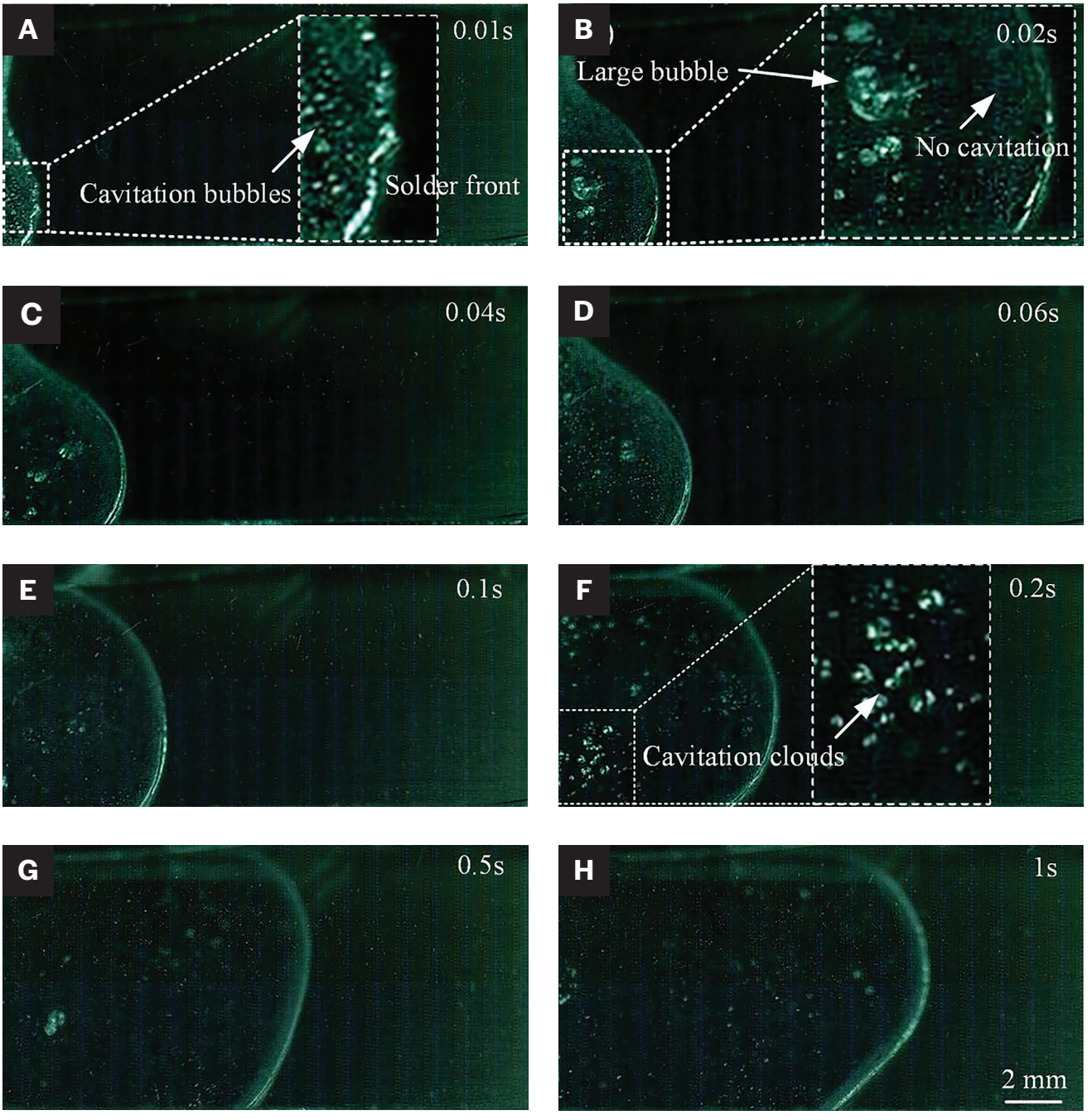

Fig. 3 — Cavitation characteristic of liquid Sn inside Al clearance at: A — 0.01 s; B — 0.02 s; C — 0.04 s; D — 0.06 s; E — 0.1 s; F — 0.2 s; G — 0.5 s; H — 1 s. Ultrasonic power was Mode I, clearance width was 0.2 mm, and the images were taken using 5000 fps.

A schematic of the simulation process is given in Fig. 2. Figure 2A shows the vibration simulation of pure Al. Such a process was realized by the ANSYS APDL 15.0 software. Therein, the solid model had the same dimension as that used in the experiment. The solid model was meshed using a grid size of 1 mm (Fig. 2A). The frequency and amplitude were the same as those used in the experiment. The lower figure in Fig. 2A shows the vibration on the substrate surface using the ultrasonic power of Mode I. Different colors represent different vibration intensities (Ref. 24). The left region of the substrate showed the same vibration intensity because such a region contacted directly with the sonotrode. Various vibrations were observed at the filling region, which can affect the filling speed of the solder.

Figure 2B shows the buildup of the filling model, which was realized by Gambit. The filling model had a length of 30 mm (1.181 in.) and a height of 3 mm. The width of the solder filling region was 20 mm. The model was meshed with grids of 0.05 mm (0.002 in.). Boundary conditions were defined after the model was built. The lower and right

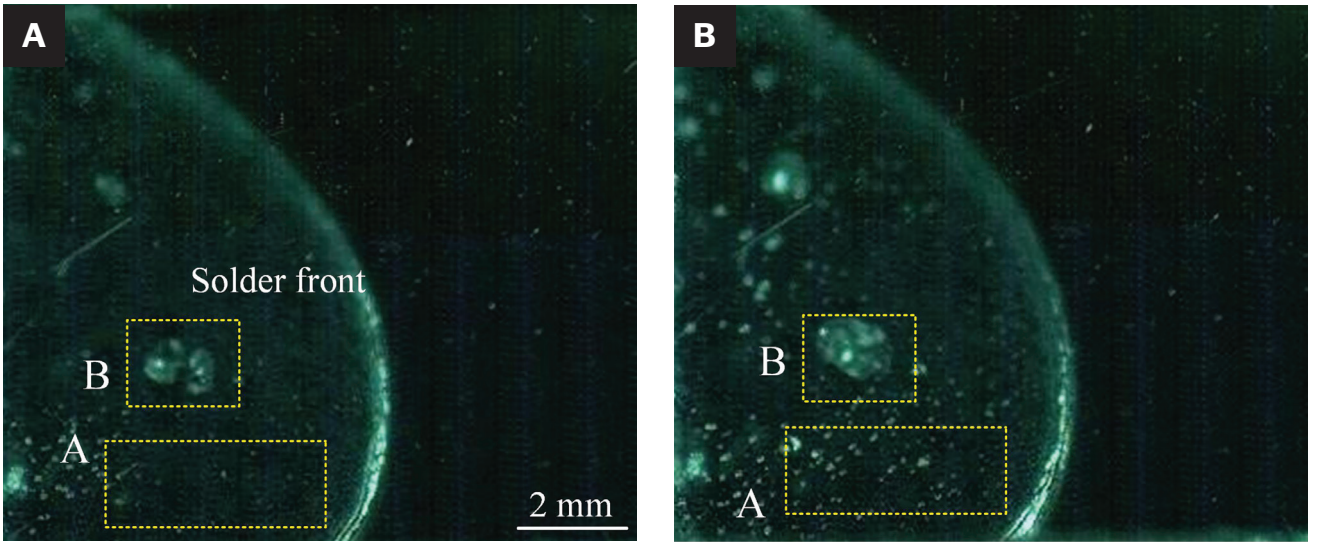

Fig. 4 — Cavitation structures of pure Sn at: A — 0.042; B — 0.042 + 200 μs (ultrasonic power was Mode I, clearance width was 0.2 mm, and the images were taken using 5000 fps).

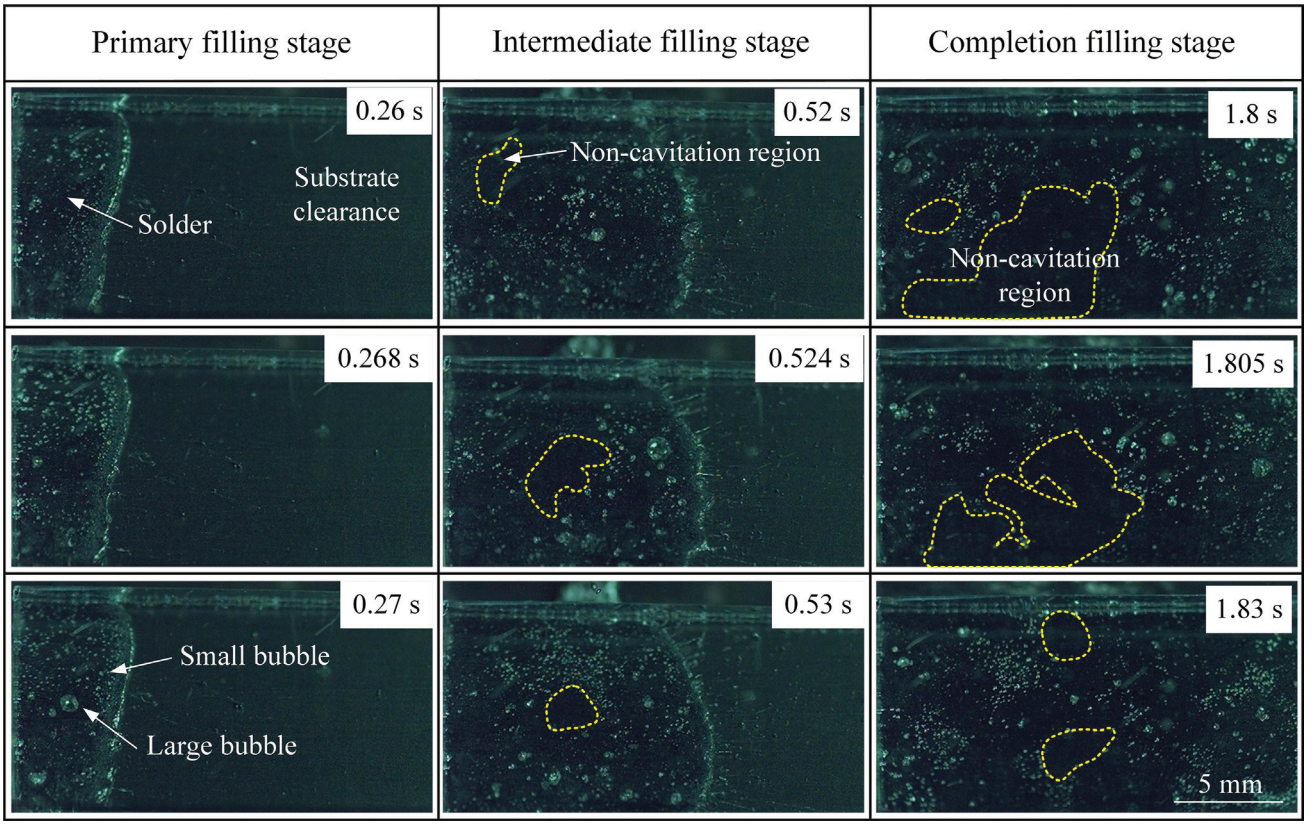

Fig. 5 — Cavitation characteristics at different filling stages (the ultrasonic power was Mode II, the clearance width was 0.2 mm, and the acquisition rate was 20,000 fps).

surfaces of the upper substrate were defined as walls. The right side of the filling clearance was defined as a pressure outlet. The upper surface of the lower substrate was defined as a vibratory wall, which was mainly used to apply vibration to the model. The left side of the filling clearance was defined as a pressure inlet.

Figure 2C shows a schematic of the simulation process. The model was exported from Gambit after the boundary conditions were defined. Then, the model was loaded in Fluent software for calculation. Some parameters were defined before the calculation, such as the density of pure Sn, 7310 kg (16,116 lb)/m^3; the surface tension of pure Sn at

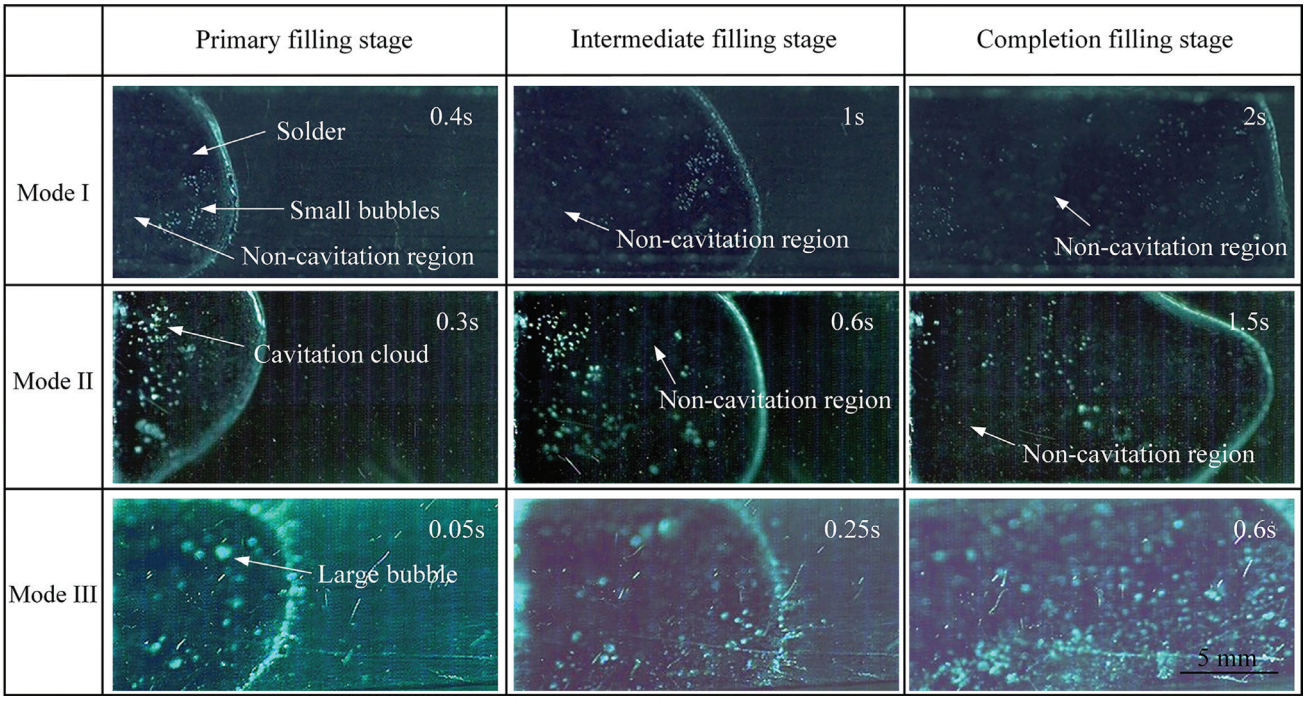

Fig. 6 — Cavitation of Sn using different ultrasonic powers (the clearance width was 0.2 mm, and the acquisition rate was 20,000 fps).

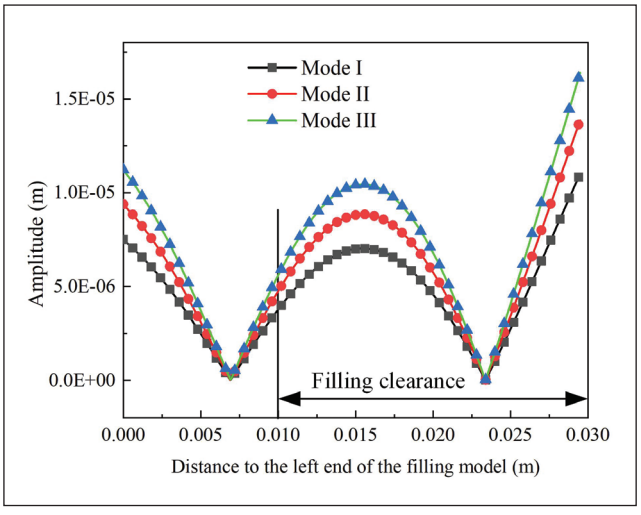

Fig. 7 — Amplitude on the substrate surface using different ultrasonic powers.

250°C, 0.556 N/m; the contacting angle of liquid Sn to pure Al, 130 deg; and the roughness of pure Al, 0.0015 mm. The VOF model was used to simulate the solder filling process. The amplitudes extracted from the substrate were applied to the vibratory wall. Fluent has a function of dynamic mesh, and the vibration condition on the substrate can be loaded on the vibratory wall by the user-defined function. After this, the soldering filling process was calculated. The calculating interval was 5 μs; namely, 1/10 of one acoustic period.

Figure 2D shows the data extraction process, which was realized in Tecplot. In this work, we mainly extracted the solder filling morphology and the acoustic pressure using different parameters.

Cavitation Characteristics and Their Affecting Factors

Cavitation Characteristics During Solder Filling

Figure 3 shows the solder filling morphologies and the cavitation characteristics at different times. The ultrasonic was operated at Mode I, the clearance width was 0.2 mm, and the images were taken using 5000 fps. The cavitation bubbles kept emerging and disappearing during the entire solder filling process. The flank and front of the solder directly contacted the air during the entire filling process. Large amounts of gas can enter the solder under the action of ultrasound, which was beneficial to the nucleation of cavitation bubbles.

As shown in Fig. 3A, numerous tiny cavitation bubbles form after 10 ms. These bubbles grow and collapse within a short time; thus, we call them "transient cavitation bubbles." Also, some bubbles oscillate and gradually grow with time, forming large bubbles (Fig. 3B). The large bubbles do not collapse after a long period (40 ms), and, thus, we call them "steady cavitation bubbles." A cavitation cloud, consisting of plenty of tiny transient cavitation bubbles, is also observed (Fig. 3F). It also forms and collapses within a short time. It is the collapse of these transient cavitation bubbles that produce micro-jets with high speeds, high pressure, and temperatures, disrupting the oxide layer of the substrate and promoting the wettability of the solder (Refs. 25, 39).

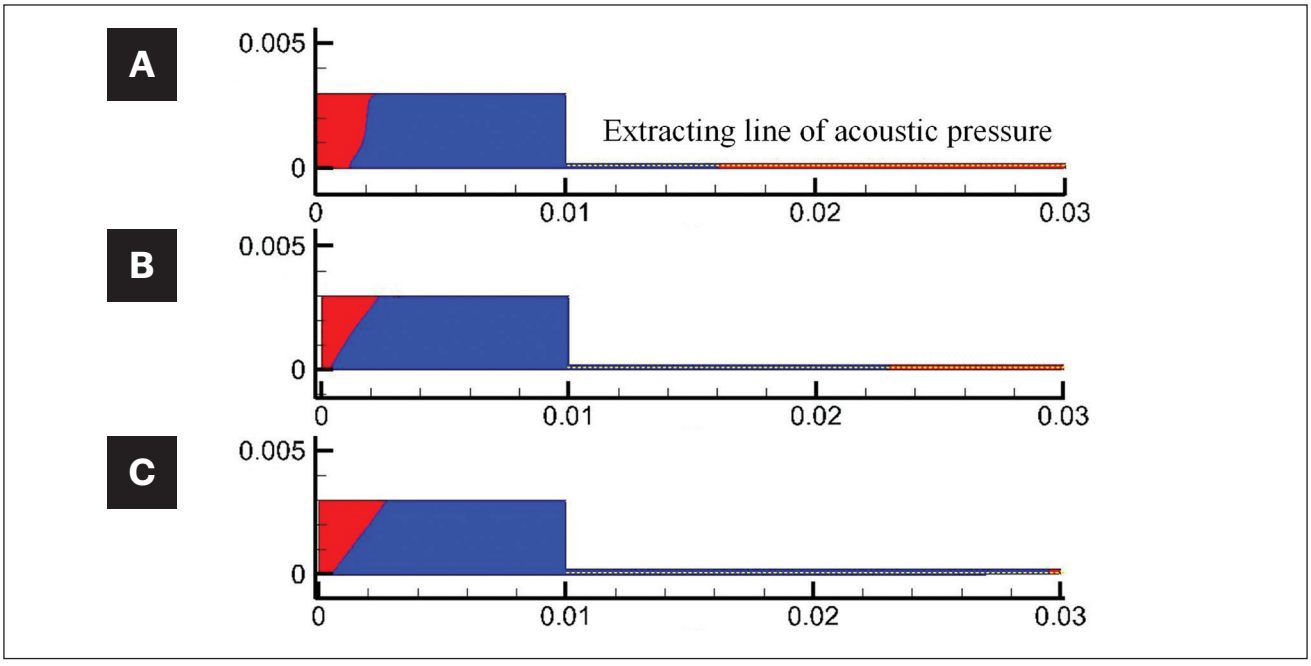

Fig. 8 — Solder filling morphologies at: A — 0.0025 s (the primary filling stage); B — 0.005 s (the intermediate filling stage); C — 0.01225 s (the completion filling stage). The clearance width was 0.2 mm, and the ultrasonic power was Mode II.

Moreover, we can see from Fig. 3 that no cavitation bubbles were observed at the solder front during the entire sonocapillary process. Such a phenomenon formed because the acoustic pressure at the solder front was below the cavitation threshold. The cavitation threshold has been reported in our previous works (Ref. 40). The acoustic pressure at the solder front will be discussed in the next section of this work.

Figure 4 shows the cavitation characteristics at two different moments with an interval of 200 µs (4 acoustic periods). The images were also taken using 5000 fps. The cavitation characteristics differed obviously at the two moments. Almost no bubbles were observed in region A at t_0. After four acoustic periods, numerous bubbles emerged (Fig. 4B). Two large bubbles were observed at region B at t_0 (Fig. 4A), and they combined to form a large bubble after 200 µs (Fig. 4B). The results of Figs. 3 and 4 show that the transient cavitation bubble and steady cavitation bubble are the two main basic cavitation structures.

To study the cavitation characteristics at different moments during the solder filling process, we divided the entire filling process into three stages: the primary filling stage, the intermediate filling stage, and the completion filling stage, as shown in Fig. 2C. The primary filling stage was defined as when the solder filled less than 40% of the substrate clearance. The intermediate filling stage was defined as when the filling distance ranged from 40% to 100%. Ultrasonic vibration continued when the entire clearance was filled. This stage was called the completion filling stage.

Figure 5 shows the cavitation characteristics at different stages. Ultrasonic power of Mode II, clearance width of 0.2 mm, and acquisition rate of 20,000 fps were used. The cavitation characteristic at three different moments were given. Some large bubbles along with numerous tiny ones were observed at the primary filling stage. These bubbles were distributed evenly in the solder. The bubble density was high. Numerous large and tiny bubbles were also observed during the intermediate filling stage. However, the bubble density showed a slight decrease. Noncavitation regions (marked by the yellow line) were observed, but they only persisted for a short time. During the completion filling stage, the size of the noncavitation regions increased. Also, the sizes and quantities of the large bubbles decreased. Most of the bubbles were transient cavitation bubbles during the completion filling stage.

Figure 5 shows that the bubbles with large sizes easily appeared at the primary filling stage, while the tiny transient bubbles preferentially appeared at the late filling stages. Such phenomena can be explained by several reasons. One, some gas nuclei can exist in the liquid solder even if it is metal (Ref. 52). Under ultrasonic, the gas nucleus can absorb the gas nearby to form a cavitation bubble. The gas content will decrease with ultrasonic time increasing, which is called "ultrasonic melt degassing" (Ref. 48). Decreased bubble density with smaller bubble sizes were obtained after the degassing process. Two, the solder front directly contacts the air during its filling process. Large amounts of gas nuclei can enter the solder under the action of ultrasound (Ref. 53). The solder gains a large filling velocity during the primary filling stage (Ref. 24), thereby causing more gas nuclei to enter the solder. Under ultrasonic, more gas nucleus is beneficial to the formation and convergence of cavitation bubbles, which contributes to the formation of large-size cavitation bubbles.

The large cavitation bubbles will oscillate and collapse with time increasing, causing some tiny gas nuclei to disperse into the solder. As a result, the quantity of the large cavitation bubbles decreases, and they evolve into transient cavita-

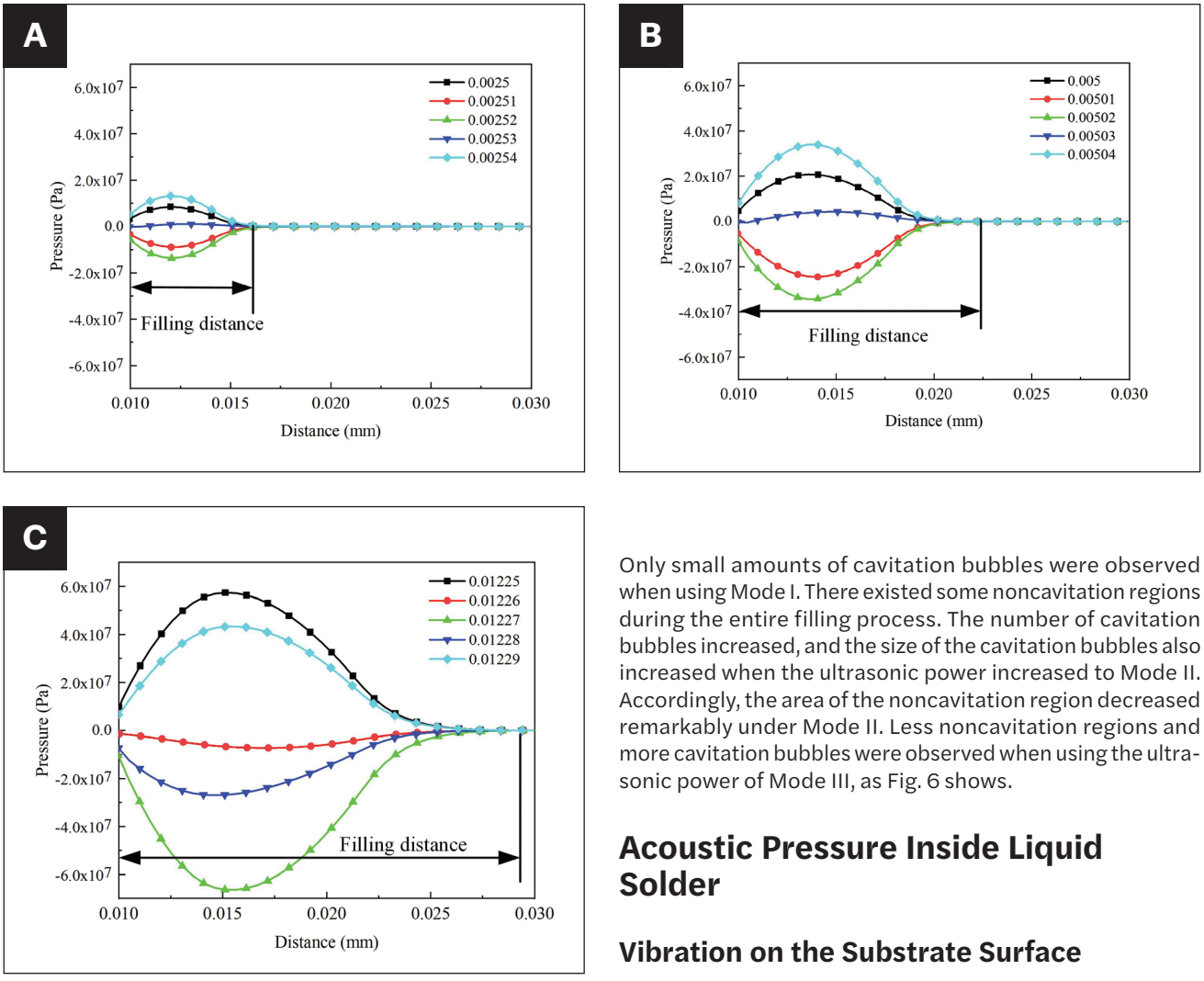

Fig. 9 — Acoustic pressure within one acoustic period at different filling stages: A — 0.0025 s – 0.00254 s, primary filling stage; B — 0.005 s – 0.00504 s, intermediate filling stage; C — 0.01225 s – 0.01229 s, completion filling stage. The clearance width was 0.2 mm, and the ultrasonic power was Mode II.

tion bubbles with small sizes as the filling process goes on. Moreover, cavitation bubbles are not evenly distributed in the solder. Some noncavitation regions are observed, and these regions change with the filling of the solder.

Effect of Ultrasonication Power on Cavitation Characteristic

Figure 6 shows the cavitation characteristics of pure Sn using different ultrasonic powers. The clearance width of 0.2 mm and the acquisition rate of 20,000 fps were used. The cavitation intensity increased obviously with increasing ultrasonic power. The number of tiny transient cavitation bubbles increased, and the large stable cavitation bubbles also tended to be larger when using higher ultrasonic power. Only small amounts of cavitation bubbles were observed when using Mode I. There existed some noncavitation regions during the entire filling process. The number of cavitation bubbles increased, and the size of the cavitation bubbles also increased when the ultrasonic power increased to Mode II. Accordingly, the area of the noncavitation region decreased remarkably under Mode II. Less noncavitation regions and more cavitation bubbles were observed when using the ultrasonic power of Mode III, as Fig. 6 shows.

Acoustic Pressure Inside Liquid Solder

Vibration on the Substrate Surface

Figure 7 shows the vibration amplitudes along the centerline of the substrate surface using different ultrasonic powers. From the clearance entrance to its end, the amplitude first increased then decreased and finally increased. The strongest vibration was obtained at the end of the clearance. Different input powers resulted in different vibration intensities, but they all had a similar variation trend. The strongest vibration was obtained when using the ultrasonic power of Mode III, while the weakest vibration was obtained when using Mode I.

Soldering Filling Process

Here, we simulated the filling process of the pure Sn solder. Figure 8 shows the filling morphologies at different filling stages. The clearance width was 0.2 mm. The ultrasonic power was Mode II. Figure 8A shows the filling morphology at 0.0025 s after the ultrasonication starts. The solder presented obvious filling inside the clearance, indicating a fast solder filling speed. Figure 8B shows the filling morphology at 0.005 s. The solder filled longer than half of the clearance. Figure 8C shows the solder filling morphology at 0.01225 s. The solder had completed the entire filling process. Thereafter, the solder showed no obvious variation.

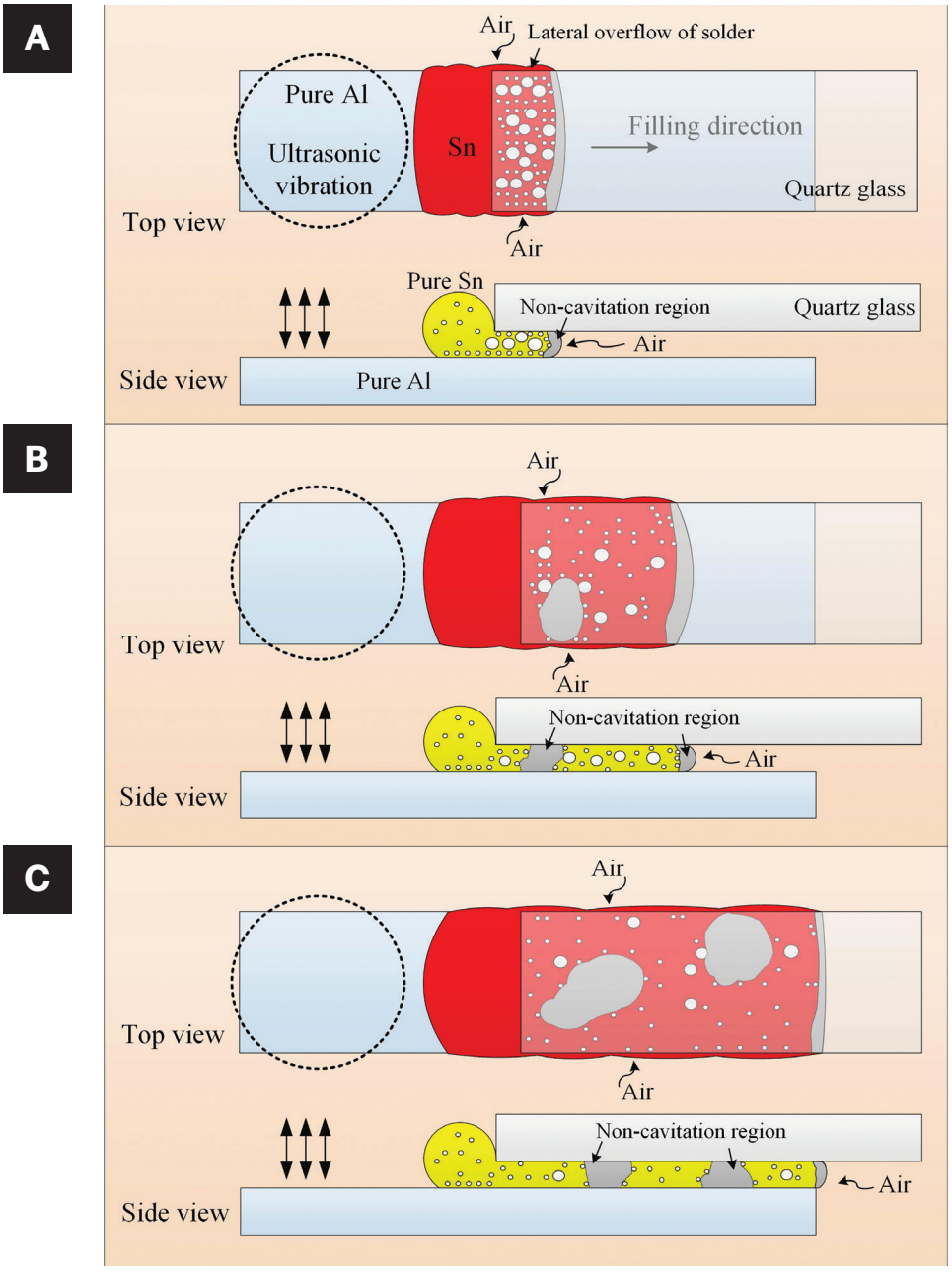

Fig. 10 — Schematic of the cavitation during the solder filling process: A — The primary filling stage; B — the intermediate filling stage; C — the completion filling stage.

Acoustic Pressure at Different Filling Stages

Since the acoustic pressure can affect the cavitation characteristics, we studied the acoustic pressure in the solder at different filling stages, and the results are given in Fig. 9. The width of the substrate clearance was 0.2 mm, and the ultrasonic power was Mode II. Figure 9A shows the pressure curves during the primary filling stage. The pressure was taken from 0.0025 s to 0.00254 s. The extracting position is shown in Fig. 8A. The maximum pressure reached 13.7 MPa at 0.00252 s. The pressure gradually decreased from the solder center to its front. The pressure decreased to the atmospheric pressure out of the solder. Fig. 9B shows the pressure curves within one period during the intermediate filling stage. The pressure was taken from 0.005 s to 0.00504 s. The extracting position is shown in Fig. 8B. Compared with the primary filling stage, higher pressures were obtained during the intermediate filling stage. The maximum pressure reached 34.4 MPa at 0.00502 s. Like the primary filling stage, the pressure gradually decreased toward the solder front and had a value close to atmospheric pressure out of the solder. Fig. 9C shows the pressure curves within one period during the completion filling stage. The pressure was taken from 0.01225 s to 0.01229 s. The pressure-extracting curve is shown in Fig. 8C. The high-

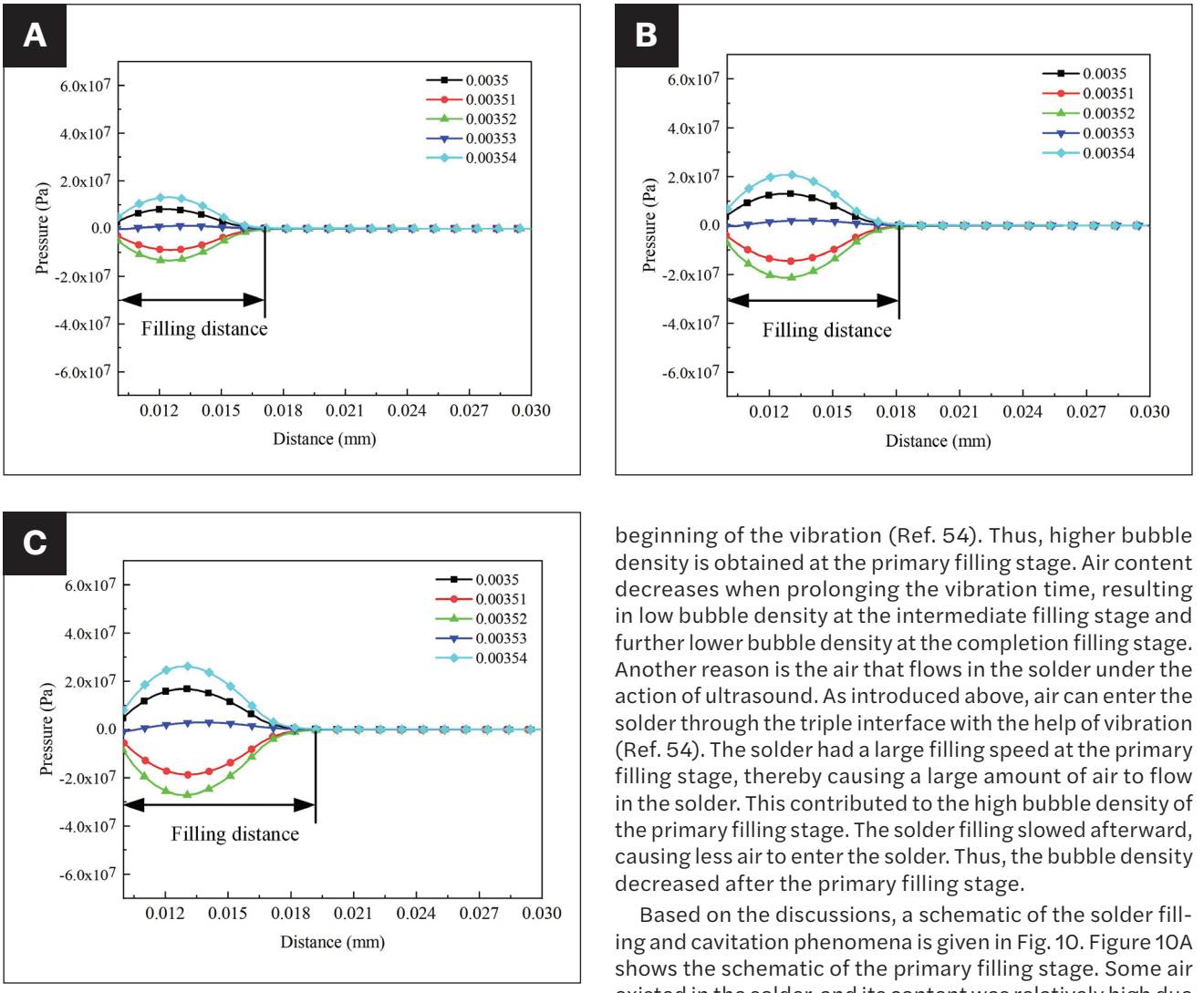

Fig. 11 — Acoustic pressure within one acoustic period 0.0035 s – 0.00354 s: A — Mode I; B — Mode II; C — Mode III.

est acoustic pressure could be obtained during this stage. The maximum value was 66.4 MPa, and it was obtained at 0.01227 s. Different from the primary and the intermediate filling stages, high pressure could be obtained inside most of the clearance. Only a small region having low acoustic pressure was obtained at the exit of the clearance because it directly contacted the air.

Figure 9 shows that the acoustic pressure in the solder was low during the primary filling stage, and it increased with the solder filling process. The pressure at the completion filling stage was nearly five times that at the primary filling stage. Such a result presented an opposite trend with the bubble density shown in Fig. 5, which shows that higher bubble density was obtained during the primary filling stage. This phenomenon can be explained by the two following reasons. The first is the air content inside the solder. The bubble density was not only determined by the acoustic pressure but also affected by the air content in the liquid. Commonly speaking, higher air content is obtained at the beginning of the vibration (Ref. 54). Thus, higher bubble density is obtained at the primary filling stage. Air content decreases when prolonging the vibration time, resulting in low bubble density at the intermediate filling stage and further lower bubble density at the completion filling stage. Another reason is the air that flows in the solder under the action of ultrasound. As introduced above, air can enter the solder through the triple interface with the help of vibration (Ref. 54). The solder had a large filling speed at the primary filling stage, thereby causing a large amount of air to flow in the solder. This contributed to the high bubble density of the primary filling stage. The solder filling slowed afterward, causing less air to enter the solder. Thus, the bubble density decreased after the primary filling stage.

Based on the discussions, a schematic of the solder filling and cavitation phenomena is given in Fig. 10. Figure 10A shows the schematic of the primary filling stage. Some air existed in the solder, and its content was relatively high due to the short ultrasonic time. Also, the solder had a large filling velocity, causing a large amount of air to enter the solder/glass interface. Thus, high bubble density was obtained at the primary filling stage. Lots of large steady bubbles and tiny transient bubbles were observed. The solder front contacted directly with the air, forming a noncavitation region. Figure 10B shows the schematic of the intermediate filling stage. The air content in the solder decreased with time increasing (degassing). A certain amount of gas was always dissolved in the liquid metal. The gas content in the solder was higher at the beginning of the vibration. At the late stage of vibration, the gas content will decrease due to the degassing effect of ultrasonic waves (Refs. 50, 54); that is, the ultrasonic wave causes the bubbles in the solder to converge, grow, and then spill out into the atmosphere. Also, the solder filling slows down, causing less air to enter the solder/glass interface. These two reasons result in low bubble density at the intermediate filling stage. The quantities of the steady bubbles and the tiny transient bubbles decrease. The noncavitation region can also be observed at the solder front, the same as the primary filling stage. Worth mentioning is that some noncavitation regions were also observed in the filled region, but they did not exist continuously. Cavitation bubbles will nucleate inside the noncavitation regions after

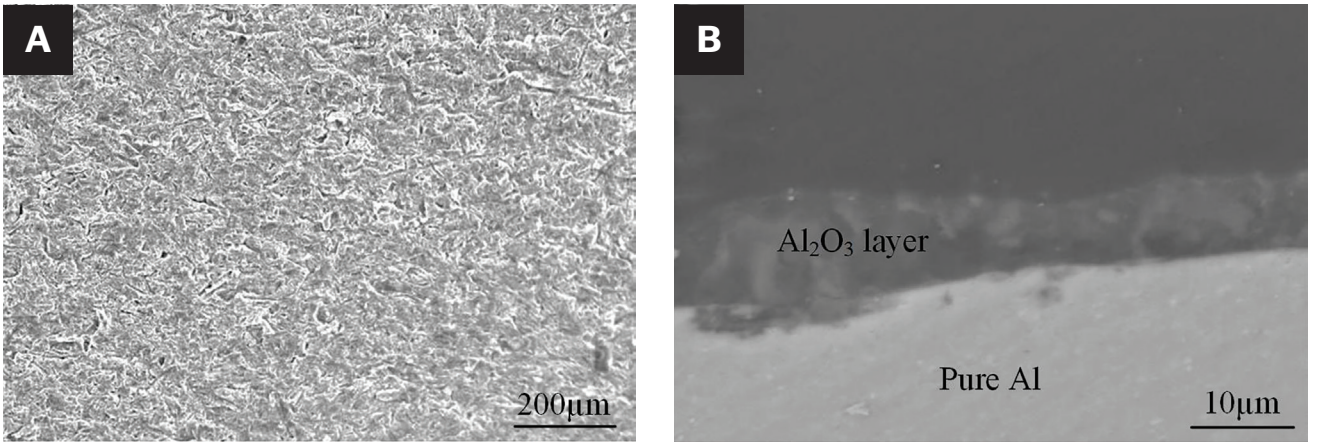

Fig. 12 — Oxide layer after anodic oxidation: A — Surface morphology; B — cross section.

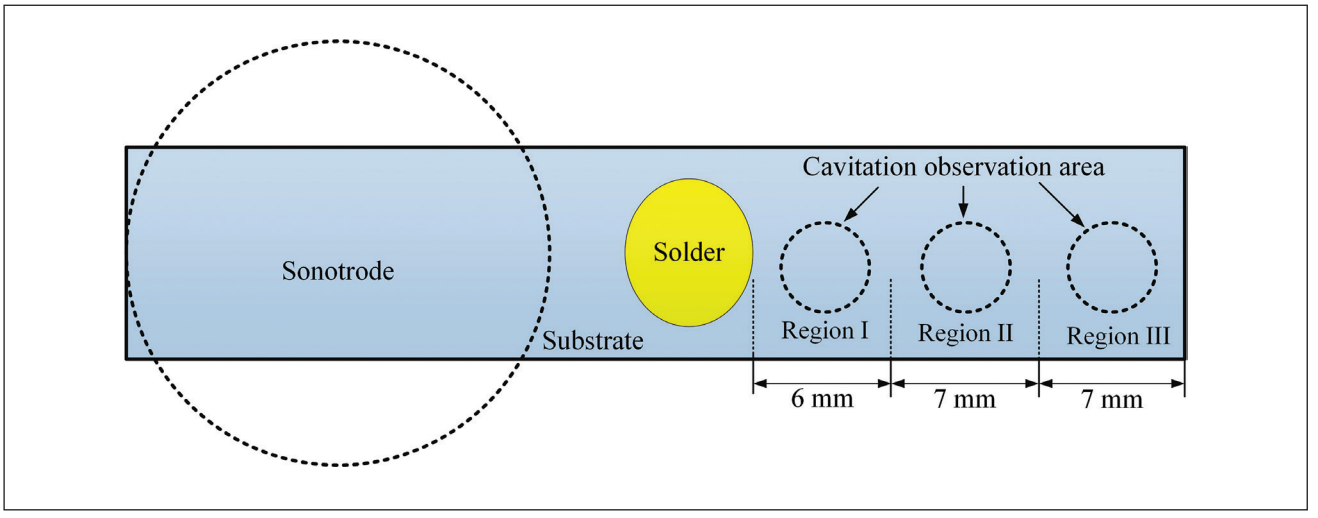

Fig. 13 — Schematic of different regions on the substrate.

a certain amount of time. Figure 10C shows the schematic of the completion filling stage. The solder filling process was accomplished. Thus, extremely low content of air could enter the solder/glass interface. Also, the original air in the solder was almost exhausted due to the long ultrasonic time. Thus, low bubble density was obtained. The cavitation field was mainly dominated by tiny transient bubbles with a few large, steady bubbles. The area of the noncavitation region increased compared with the primary filling stage and the intermediate filling stage.

Acoustic Pressure During Different Ultrasonic Powers

Figure 6 shows that ultrasonic power has an obvious effect on the cavitation characteristic. Thus, we studied the acoustic pressure in the solder using different ultrasonic powers. All the pressure values were extracted from 0.0035 s to 0.00354 s. Figure 11A shows the pressure curves using Mode I. The maximum acoustic pressure reached 13.2 MPa at 0.00354 s. The filling distance was quite small, with a value of approximately 0.017 m (0.056 ft). Fig. 11B shows the pressure curves using Mode II. The pressure amplitude increases and the maximum value could reach 20.7 MPa. Accordingly, the filling distance increased, and it had a value of approximately 0.018 m (0.059 ft). The pressure curves using Mode III are shown in Fig. 11C. The maximum acoustic pressure reached 26.2 MPa, and the filling distance reached approximately 0.019 m (0.062 ft). Fig. 11 shows that higher acoustic pressure can be obtained when using higher ultrasonic power, corresponding well with the higher bubble intensity shown in Fig. 6. Also, a large filling distance can be obtained when using higher ultrasonic power, which has been reported in one of our previous works (Ref. 24).

Cavitation Erosion of Substrate

Oxide Layer, Division of Different Erosion Regions

Figure 12 shows the oxide layer on the substrate surface after oxidation. Figure 12A shows the surface morphology of the oxide layer. The oxide layer had some tiny cracks. Figure

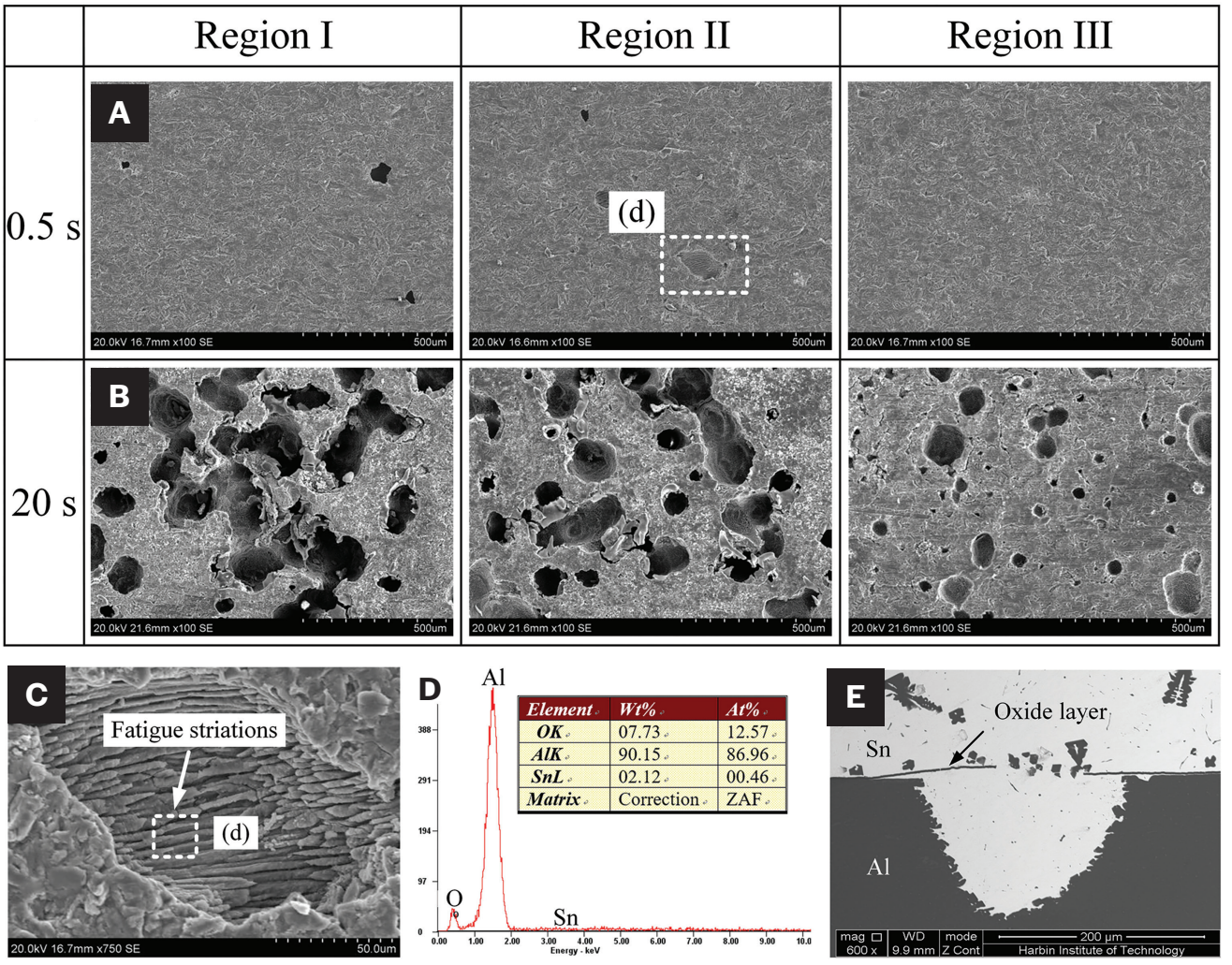

Fig. 14 — Erosion morphologies on the substrate using ultrasonication time of: A — 0.5 s; B — 20 s; C — fatigue striations; D — EDS result of the erosion pit; E — cross section of an erosion pit.

12B shows the cross section of the oxide layer. It presented a relatively darker color compared with pure Al. The thickness of the oxide layer was 5–10 µm.

The solder filled into the substrate clearance and then advanced toward the other end under ultrasonication. Cavitation inside the clearance was intense, and the oxide layer on the substrate could be removed within a short time. The primary-filled region undoubtedly underwent a longer erosion time than the intermediate-filled region. Thus, different erosion effects could be obtained at different filled regions. To make the comparison easier, we divided the substrate into three regions, as shown in Fig. 13. Three different regions are marked, and they had a width of 6 mm (0.236 in.), 7 mm (0.275 in.), and 7 mm, respectively.

Morphology of Eroded Surface Under Ultrasonication

Figure 14A shows the morphologies of the eroded substrate after the ultrasonic time of 0.5 s. The ultrasonic power was Mode II. Only several erosion pits were observed in Region I. The erosion pit presented irregular edges. The diameter of the erosion pit was approximately 50 µm. A similar morphology was observed in Region II, but the depths of the erosion pits were smaller (showing lighter color). A magnified view of the erosion pit showed obvious fatigue ripples, indicating that the cavitation erosion mechanism was fatigue (Fig. 14C). This result corresponds well with the work of Abouel-Kasem et al. (Ref. 55). Almost no erosion pit was observed at Region III because the oxide layer was not broken under a short ultrasonication time. Figure 14B shows the erosion morphologies after 20 s. More erosion pits were observed at all regions, indicating that longer ultrasonic time is beneficial to the erosion effect. Some erosion pits contacted each other at regions I and II, indicating the complete removal of the oxide layer. Plenty of erosion pits were observed in Region III, showing a more obvious erosion effect than those using short times. An energy-dispersive x-ray spectrometer (EDS) was performed on the erosion pit. The result in Fig. 14D shows that the main elements were Al (89.96 at.-%) and O (12.57 at.-%), indicating that the oxide layer was removed in the erosion pit. Figure

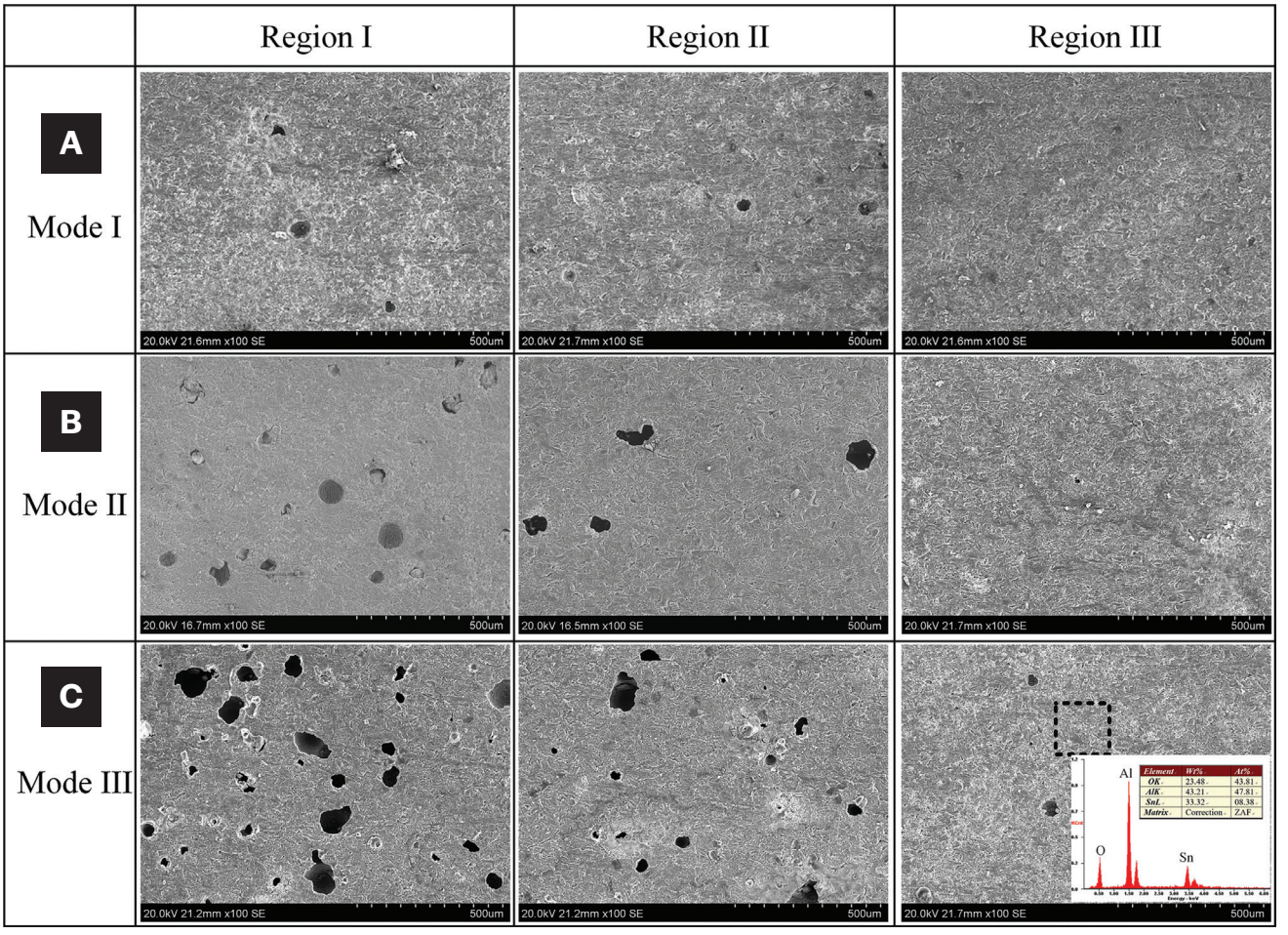

Fig. 15 — Erosion morphologies on the substrate using ultrasonication power of: A — Mode I; B — Mode II; C — Mode III.

14E shows the cross-section morphology of an erosion pit, showing that the surface pit of Al substrate was an indication of oxide removal. Figure 14 shows that ultrasonic time can greatly affect the erosion effect, and longer time causes a better erosion effect.

Effect of Ultrasonic Power on the Erosion Effect

Figure 15 shows the erosion morphologies on the substrate using different ultrasonic powers. The ultrasonic time was 2 s. Figure 15A shows the erosion morphologies using Mode I. Weak erosion was observed on the entire substrate. Only three erosion pits were observed in Region I. Similarly, only several erosion pits were observed in Region II, but their sizes were smaller. No erosion pit was observed at Region III, which was like that using a short time of 0.5 s. Figure 15B shows the erosion morphologies using the ultrasonic power of Mode II. Much more obvious erosion was observed compared with that using Mode I. Figure 15C shows the erosion morphologies using the ultrasonic power of Mode III. More erosion pits with larger sizes were observed, indicating that high ultrasonic power is beneficial to the erosion effect. Numerous erosion pits were observed in Region I, and they had have large depths and showed dark color. Region II had fewer erosion pits than Region I but more erosion pits compared with that using Mode I and II. Several erosion pits were observed in Region III. An energy dispersive x-ray spectrometer (EDS) was used in the region where no erosion pits were observed. The result shows that the main elements were Al (47.81% at) and O (43.81% at), indicating an intact oxide layer. As shown in Fig. 6, much higher cavitation intensity was observed when using higher ultrasonic power. The collapse of more cavitation bubbles can cause pronounced erosion on the substrate. In conclusion, the results in Figs. 6 and 15 show that ultrasonic power is an important factor affecting erosion, and stronger erosion is obtained when using higher ultrasonic power.

Summary of This Work

A comparison of the solder filling speeds from the simulations and experiments was made in Fig. 8 (1632 mm [64 in.]/s) and Fig. 5 (11 mm [0.433 in.]/s). We can see that the solder filling speeds during the actual experiments were much smaller than those obtained from the simulation. This can be attributed to two reasons: 1. During actual soldering, the solder must break the oxide layer on its front to achieve the filling process. Such a process requires a period of ultrasonic action time,

making the filling behavior slow; 2. During actual soldering, obvious lateral overflow of the solder can be observed (Ref. 24). Such a process will cause insufficient solder at the filling front. A 2D model was used during the simulation, which did not need to consider this problem. Further study is needed to understand the cause of the discrepancy and to improve the model.

However, the simulation in this work was used to predict the filling trend under different parameters. Another function is that it can illustrate the effect of parameters on the acoustic pressure of the solder and further prove the change of cavitation.

Joint clearance is one of the most important soldering parameters for ultrasonic soldering. Changing the joint clearance can change the acoustic pressure in solders, thereby changing the cavitation intensity (Ref. 25) and solder filling speed (Ref. 24). The impact of joint clearance on the soldering process is not discussed here and will be reported in future work.

Conclusions

In this work, the cavitation characteristics during the sonocapillary action of ultrasonic soldering were studied by high-speed photography. The bubble types were defined, and the effects of soldering parameters such as ultrasonic power and substrate clearance on the cavitation characteristics and their erosion effects were studied. The following conclusions can be drawn.

1. Cavitation occurs during the entire sonocapillary process. Tiny transient cavitation bubbles and large steady cavitation bubbles are the main bubble types. Transient cavitation bubbles can nucleate and collapse within a short time, while steady cavitation bubbles constantly oscillate and drift and have longer life.

2. The sonocapillary action is divided into the primary filling stage, the intermediate filling stage, and the completion filling stage. Different cavitation characteristics were observed at different stages. Tiny transient bubbles dominated the cavitation field at the completion filling stage. The primary filling stage had higher bubble density even though it had low ultrasonic pressure because the air content in the solder was high.

3. Higher ultrasonic power results in higher acoustic pressure and, therefore, stronger cavitation in the solder. Cavitation intensity directly affects the erosion effect on the substrate. Higher ultrasonic power causes a better erosion effect. Longer ultrasonic time also results in a better erosion effect.

Acknowledgments

Project funded by National Natural Science Foundation of China (No. 52305350), New Era Excellent Master's and Doctor's thesis of Heilongjiang Province (LJYXL2022-043), Natural Science Foundation of Chongqing (No. CSTB2023NSCQ-MSX0638), China Postdoctoral Science Foundation (2022M710937), and Hei Long Jiang Postdoctoral Foundation (No. LBH-Z22026).

References

1. Hunicke, R. L. 1976. Ultrasonic soldering pots for fluxless production soldering. *Welding Journal* 55(3): 191–194.

2. Saxty, P. 1999. Ultrasonic soldering–a farewell to flux. *Welding and Metal Fabrication* 67(3): 15–17.

3. Ding, M., Zhang, P., Zhang, Z., and Yao, S. 2010. Direct-soldering 6061 aluminum alloys with ultrasonic coating. *Ultrasonics Sonochemistry* 17: 292–297.

4. Ji, H., Li, L., Wang, L., and Li, M. 2015. Microstructures and properties of the Fe-based amorphous foil/aluminum dissimilar joint by ultrasonic-assisted soldering. *Welding in the World* 59: 623–628.

5. Lai, Z., Chen, X., Pan, C., Xie, R., Liu, L., and Zou, G. 2016. Joining Mg alloys with Zn interlayer by novel ultrasonic-assisted transient liquid phase bonding method in air. *Materials Letters* 166: 219–222.

6. Lai, Z., Xie, R., Pan, C., Chen, X., Liu, L., Wang, W., and Zou, G. 2017. Ultrasound-assisted transient liquid phase bonding of magnesium alloy using brass interlayer in air. *Journal of Materials Science & Technology* 33: 567–572.

7. Tillmann, W., Zimpel, M., Dias, N. F. L., Pfeiffer, J., Wojarski, L., and Xu, Z. 2015. Mechanical and microstructural analysis of ultrasonically assisted induction-brazed TiAl6V4 joints. *Welding in the World* 59: 901–909.

8. Wielage, B., Hoyer, I., and Weis, S. 2007. Soldering aluminum matrix composites. *Welding Journal* 86(3): 67–70.

9. Xu, Z., Yan, J., Wu, G., Kong, X., and Yang, S. 2005. Interface structure and strength of ultrasonic vibration liquid phase bonded joints of Al_2O_3/6061Al composites. *Scripta Materialia* 53(7): 835–839.

10. Ji, H., Cheng, X., and Li, M. 2016. Ultrafast ultrasonic-assisted joining of bare α-alumina ceramics through reaction wetting by aluminum filler in air. *Journal of the European Ceramic Society* 36: 4339–4344.

11. Kostolný, I., Koleňák, R., Hodúlová, E., Zacková, P., and Kusý, M. 2019. Investigation of ultrasound-assisted soldering of SiC ceramics by Zn-Al-In high-temperature solder. *Welding in the World* 63: 1449–1459.

12. Koleňák, R., Kostolný, I., Drápala, J., Sahul, M., and Urminský, J. 2018. Characterizing the soldering alloy type In–Ag–Ti and the study of direct soldering of SiC ceramics and copper. *Metals* 8: 274.

13. Wilson, C., Thompson, L., Choi, H., and Bostwick, J. B. 2021. Enhanced wettability in ultrasonic-assisted soldering to glass substrates. *Journal of Manufacturing Processes* 64: 276–284.

14. Cui, W., Yan, J., Dai, Y., and Li, D. 2015. Building a nano-crystalline α-alumina layer at a liquid metal/sapphire interface by ultrasound. *Ultrasonics Sonochemistry* 22: 108–112.

15. Yu, W., Liu, S., Liu, X., Liu, M., and Shi, W. 2015. Interface reaction in ultrasonic vibration-assisted soldering of aluminum to graphite using Sn–Ag–Ti solder foil. *Journal of Materials Processing Technology* 221: 285–290.

16. Jenkins, W. B. 1976. Fluxless soldering of aluminum heat exchangers. *Welding Journal* 55(1): 28–35.

17. Gunkel, R. W. 1979. Solder aluminum joints ultrasonically. *Welding Design & Fabrication* 58(9): 90–92.

18. Tamura, S., Tsunekawa, Y., Okumiya, M., and Hatakeyama, M. 2008. Ultrasonic cavitation treatment for soldering on Zr-based bulk metallic glass. *Journal of Materials Processing Technology* 206(1): 322–327.

19. Lanin, V. L. 2001. Ultrasonic soldering in electronics. *Ultrasonics Sonochemistry* 8: 379–385.

20. Graff, K. 2007. Ultrasonic soldering and brazing. *EWI Insights*.

21. Dong, F., Li, X., Zhang, L., Ma, L., and Li, R. 2016. Cavitation erosion mechanism of titanium alloy radiation rods in aluminum melt. *Ultrasonics Sonochemistry* 31: 150–156.

22. Yan, J., Zhao, W., Xu, H., Li, D., Xu, Z., Yang, S., Zhang, Y., and Ma, Z. 2009. Ultrasonic brazing of aluminum alloy and aluminum matrix composite. US Patent 7624906B2, filed November 21, 2007, and issued December 1, 2009.

23. Zhao, W., Yan, J., Yang, W., and Yang, S. 2008. Capillary filling process during ultrasonically soldering of aluminium matrix composites. *Science and Technology of Welding and Joining* 13(1): 66–72.

24. Xu, Z., Li, Z., Ma, L., Cao, Z., Yang, J., and Yan, J. 2019. Dynamic behavior of solder filling during ultrasonic soldering. *Welding Journal* 98: 194–203.

25. Li, Z., Xu, Z., Ma, L., Wang, S., Liu, X., and Yan, J. 2018. Cavitation at filler metal/substrate interface during ultrasonic-assisted soldering. Part I: Cavitation characteristics. *Ultrasonics Sonochemistry* 49: 249–259.

26. Virot, M., Chave, T., Nikitenko, S. I., Shchukin, D. G., Zemb, T., and Moehwald, H. 2010. Acoustic cavitation at the water-glass interface. *The Journal of Physical Chemistry C* 114: 13083–13091.

27. Tzanakis, I., Xu, W., Lebon, G., Eskin, D., Pericleous, K., and Lee, P. 2015. In situ synchrotron radiography and spectrum analysis of transient cavitation bubbles in molten aluminium alloy. *Physics Procedia* 70: 841–845.

28. Suslick, K. S., Didenko, Y., Fang, M. M., Hyeon, T., Kolbeck, K. J., McNamara III, W. B., Mdleleni, M. M., and Wong, M. 1999. Acoustic cavitation and its chemical consequences. *Philosophical Transactions of the Royal Society* 357: 335-353.

29. Moussatov, A., Granger, C., and Dubus, B. 2005. Ultrasonic cavitation in thin liquid layers. *Ultrasonics Sonochemistry* 12: 415–422.

30. Niazi, S., Hashemabadi, S. H., and Razi, M. M. 2014. CFD simulation of acoustic cavitation in a crude oil upgrading sonoreactor and prediction of collapse temperature and pressure of a cavitation bubble. *Chemical Engineering Research & Design* 92: 166–173.

31. Kim, K. Y., Byun, K., and Kwak, H. 2007. Temperature and pressure fields due to collapsing bubble under ultrasound. *Chemical Engineering Journal* 132: 125–135.

32. Flint, E. B., and Suslick, K. S. 1991. The temperature of cavitation. *Science* 20: 1397–1399.

33. Kim, K. Y., Byun, K., and Kwak, H. 2007. Temperature and pressure fields due to collapsing bubble under ultrasound. *Chemical Engineering Journal* 132: 125–135.

34. Brujan, E. A., Ikeda, T., and Matsumoto, Y. 2008. On the pressure of cavitation bubbles. *Experimental Thermal and Fluid Science* 32: 1188–1191.

35. Brujan, E., and Matsumoto, Y. 2012. Collapse of micrometer-sized cavitation bubbles near a rigid boundary. *Microfluidics and Nanofluidics* 13: 957–966.

36. Shuai, L., Yun-bo, L., and A-man, Z. 2015. Numerical analysis of the bubble jet impact on a rigid wall. *Applied Ocean Research* 50: 227–236.

37. Suslick, K. S. 1989. The chemical effects of ultrasound. *Scientific American* February: 80–89.

38. Chen, H., and Liu, S. 2009. Inelastic damages by stress wave on steel surface at the incubation stage of vibration cavitation erosion. *Wear* 266: 69–75.

39. Li, Z., Xu, Z., Ma, L., Wang, S., Liu, X., and Yan, J. 2019. Cavitation at filler metal/substrate interface during ultrasonic-assisted soldering. Part II: cavitation erosion effect. *Ultrasonics Sonochemistry* 50: 278–288.

40. Li, Z., Xu, Z., He, P., Ma, Z., Chen, S., and Yan, J. 2022. Dependence of wetting on cavitation during the spreading of a filler droplet on the ultrasonically agitated Al substrate. *Ultrasonics Sonochemistry* 82: 105893.

41. Li, Y., Chen, C., and Yi, R. 2021. Recent development of ultrasonic brazing. *International Journal of Advanced Manufacturing Technology* 114: 27–62.

42. Min, D. 2019. Ultrasonic semi-solid soldering 6061 aluminum alloys joint with Sn-9Zn solder reinforced with nano/nano+micron Al_2O_3 particles. *Ultrasonics Sonochemistry* 52: 150–156.

43. Lv, J., Xiao, Y., Liu, B., Li, B., Zhang, J., Sun, S., and Luo, D. 2022. Microstructure evolution and interfacial bonding mechanisms of ultrasonically soldered sapphire/Al dissimilar joints using Sn-based solders. *Ceramics International* 48(14): 20070–20077.

44. Yi, X., Zhang, R., and Hu, X. 2021. Study on the microstructure and mechanical property of Cu-foam modified Sn3.0Ag0.5Cu solder joints by ultrasonic-assisted soldering. *Journal of Manufacturing Processes* 64: 508–517.

45. Li, Z., Xu, Z., He, P., Ma, Z., Chen, S., and Yan, J. 2022. High speed imaging and numerical simulations of cavitation characteristic during the spreading of GaIn melt under ultrasonication. *International Journal of Mechanical Sciences* 221: 107221.

46. Huang, H., Shu, D., Fu, Y., Wang, J., and Sun, B. 2014. Synchrotron radiation X-ray imaging of cavitation bubbles in Al–Cu alloy melt. *Ultrasonics Sonochemistry* 21: 1275–1278.

47. Mirihanage, W., Xu, W., Tamayo-Ariztondo, J., Eskin, D., Garcia-Fernandez, M., Srirangam, P., and Lee, P. 2016. Synchrotron radiographic studies of ultrasonic melt processing of metal matrix nanocomposites. *Materials Letters* 164: 484–487.

48. Xu, W., Tzanakis, I., Srirangam, P., Mirihanage, W., Eskin, D., Bodey, A., and Lee, P. 2016. Synchrotron quantification of ultrasound cavitation and bubble dynamics in Al–10Cu melts. *Ultrasonics Sonochemistry* 31: 355–361.

49. Tan, D., Lee, T., Khong, J., Connolley, T., Fezzaa, K., and Mi, J. 2015. High-speed synchrotron X-ray imaging studies of the ultrasound shockwave and enhanced flow during metal solidification processes. *Metallurgical and Materials Transactions A* 46(7): 2851–2861.

50. Wang, B., Tan, D., Lee, T. L., Khong, J. C., Wang, F., Eskin, D., Connolley, T., Fezzaa, K., and Mi, J. 2018. Ultrafast synchrotron X-ray imaging studies of microstructure fragmentation in solidification under ultrasound. *Acta Materialia* 144: 505–515.

51. Mi, J., Tan, D., and Lee, T. 2015. In Situ Synchrotron X-ray study of ultrasound cavitation and its effect on solidification microstructures. *Metallurgical and Materials Transactions B* 46: 1615–1619.

52. Eskin, D. G., Al-Helal, K., and Tzanakis, I. 2015. Application of a plate sonotrode to ultrasonic degassing of aluminum melt: Acoustic measurements and feasibility study. *Journal of Materials Processing Technology* 222: 148–154.

53. Dong, H., Li, Z., Song, X., Guo, X., Luo, Y., Bai, T., Wei, S., Zhao, H., Yan, J., and Feng, J. 2019. Low temperature ultrasound-activated joining of ZrO_2 ceramics using Sn–Al–Cu solder. *Journal of the American Ceramic Society* 102: 2272–2277.

54. Xu, H., Han, Q., and Meek, T. T. 2008. Effects of ultrasonic vibration on degassing of aluminum alloys. *Materials Science and Engineering: A* 473: 96–104.

55. Abouel-Kasem, A., and Ahmed, S. M. 2012. Bubble structures between two walls in ultrasonic cavitation erosion. *Journal of Tribology* 134(2): 021702.

ZHENGWEI LI, **ZHIWU XU** (*xuzw@hit.edu.cn*), **BO ZHANG**, and **JIUCHUN YAN** are with the State Key Laboratory of Advanced Welding and Joining, Harbin Institute of Technology, Harbin, China. **LI** is also with the Chongqing Research Institute, Harbin Institute of Technology, Chongqing, China.